

Plasma molding over deep trenches and the resulting ion and energetic neutral distributions

Doosik Kim and Demetre J. Economou^{a)}

Plasma Processing Laboratory, Department of Chemical Engineering, University of Houston, Houston, Texas 77204-4004

(Received 24 September 2002; accepted 17 March 2003; published 16 June 2003)

A two-dimensional fluid/Monte Carlo simulation was developed to study plasma molding over deep trenches and the resulting ion and energetic (fast) neutral distributions, with emphasis on neutral beam sources. Plasma molding occurs when the sheath thickness is comparable to or smaller than the trench width. Using the electric field profiles predicted by the self-consistent fluid simulation, ions and energetic neutrals (resulting mainly by ion neutralization on the sidewall) were followed by the Monte Carlo simulation. The dominant energetic species at the bottom of a high aspect ratio trench were neutrals. A thin sheath (compared to the trench width), favored a larger energetic neutral flux at the bottom, at the expense of neutral energy and directionality. A relatively thick sheath produced neutrals of higher directionality at the expense of neutral flux. Neutral energy and directionality both increased by increasing the sheath potential. © 2003 American Vacuum Society. [DOI: 10.1116/1.1574049]

I. INTRODUCTION

A sheath forms over any wall in contact with plasma. The sheath over a homogeneous, flat, infinite surface is correspondingly planar (one-dimensional). When the surface contains geometrical features, however, the sheath will try to wrap around the contour of the features. This is called *plasma molding*. The important length scales that control behavior are the plasma sheath thickness, L_{sh} , and the size of surface features, for example, the width of a trench, D . When $L_{sh} \leq D$, i.e., the sheath thickness is much smaller than the trench width, the plasma–sheath interface (meniscus) will conform to the shape of the surface topography. At the other extreme, $L_{sh} \gg D$, the plasma sheath will be essentially planar as if the trench were nonexistent. The plasma simply does not feel the presence of the surface topography. This situation is encountered in microelectronics, where the feature size is below a micron while the sheath is at least 100s of microns thick. In the intermediate case, $L_{sh} \sim D$, the plasma–sheath meniscus will “bend” gently over the trench mouth becoming planar away from the feature. This situation may be encountered in MEMS fabrication,¹ ion extraction from a plasma through grids,² plasma thrusters, and neutral beam sources.³ The depth of the trench H (or aspect ratio $\equiv H/D$) is another important parameter which affects ion flow inside the trench. Plasma molding affects the flux, energy, and angular distributions of ions bombarding the surface contour, and in turn the reaction (etching or deposition) rate along the contour.

Energetic neutrals can also result due to plasma molding. Vertically collimated ions, for example, may be diverted by the existence of horizontal electric field components near the trench mouth. Such ions can strike the sidewall of the trench and reflect as energetic (fast) neutrals. The fraction of ion

energy retained by the reflected neutrals will depend on the wall material and the angle of ion impact. The omnipresent angular dispersion of ions coming from a plasma also helps in producing energetic neutrals by collisions with the sidewall.

Energetic neutrals may be used for semiconductor manufacturing to mitigate the effects of charging damage.^{4,5} A kind of energetic neutral beam source was described in Ref. 3. Ions were accelerated in the sheath and extracted from a high density plasma through a metal grid with high aspect ratio holes. It was hypothesized that ions suffered grazing angle collisions with the inner walls of the holes turning into energetic neutrals. A similar neutral beam source concept was described in Ref. 6. Plasma molding over the holes and the angular dispersion of ions play an important role in such sources.

The present work focuses on high density Ar plasma molding over a trench with high aspect ratio and the resulting ion and energetic neutral distributions. Emphasis is placed on energetic neutrals for neutral beam source applications. Previous studies addressed plasma molding over steps^{7,8} and trenches,⁹ focusing on ion distributions. The simulation described below was validated with experimental data on ion flux, energy, and angular distributions along the substrate surface, in the presence of plasma molding over the surface.

II. SIMULATION PROCEDURES

A combined fluid/Monte Carlo simulation was used. The self-consistent fluid simulation predicted the two-dimensional profiles of ion density, ion fluid velocity, and electric field in the sheath over the surface feature. The electric field profiles were then used in the Monte Carlo simulation to predict the ion (and energetic neutral) energy and angular distributions along the contour of the feature. Due to the low operating pressure, charge exchange in the gas phase

^{a)}Author to whom correspondence should be addressed; electronic mail: economou@uh.edu

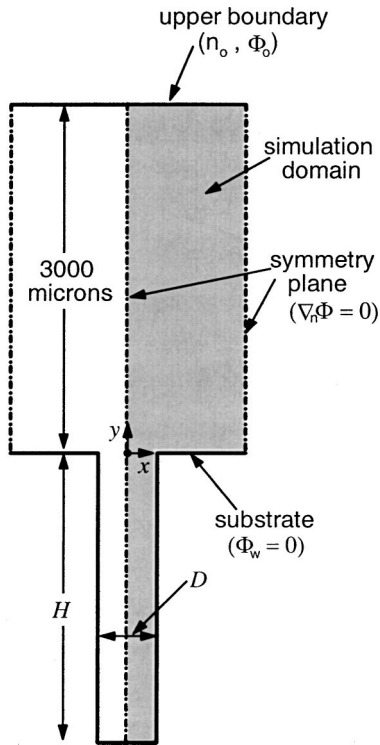


FIG. 1. Domain and boundary conditions used in the simulation. A two-dimensional deep trench is located on a conducting Fe substrate. A $500\ \mu\text{m}$ wide and $2500\ \mu\text{m}$ deep trench is shown here. Half of the domain (between two symmetry planes) was simulated. The plasma density and the electric potential were specified at the upper boundary. The wall was grounded ($\Phi_w = 0\ \text{V}$).

is not likely to occur. Thus energetic neutrals resulted mainly by ion neutralization on the sidewalls of the trench. The simulation procedures are summarized below. Details have been given in previous publications.^{7–9}

A. Fluid simulation

The two-dimensional compressible, inviscid fluid equations for ions (species and momentum balances) coupled with Poisson's equation for the electric potential were employed.^{8,10} Ions were accelerated in the sheath to achieve supersonic speeds. Electrons were assumed to be in Boltzmann equilibrium with the field, and the electron temperature T_e and background gas pressure and temperature (e.g., neutral density) were assumed to be spatially uniform. A finite difference scheme based on the flux corrected transport method¹¹ was implemented to solve the ion continuity equations. This method is conservative and transportive. It can also capture steep gradients of supersonic ion flow. The equations were integrated in time by a second-order Adams–Bashforth method. The time step was chosen so that the Courant–Friederichs–Levy condition was satisfied. At each time step, Poisson's equation was solved iteratively to update the electric potential profile. The self-consistent simulation evolved until a steady-state was reached.

The system employed in this study is shown in Fig. 1. A conductive substrate (Fe in this case) with a deep trench (width D and depth H) is located at the bottom of the do-

main. The potential was specified on the substrate (Φ_w) and at the upper boundary (Φ_o), while the sides were symmetry planes ($\nabla_n \Phi = 0$). At the upper boundary, the argon ion density (n_o) and electron temperature were also specified. Note that the electron density was set equal to the ion density at the upper boundary, in accordance with the quasi-neutral plasma approximation. The plasma sheath (where charge neutrality breaks down) evolved self-consistently, provided that the upper boundary of the domain was several times thicker than the sheath. Larger electron (ion) densities and lower electron temperatures (smaller Debye lengths) result in thinner sheaths (for a given sheath potential). Actual neutral beam sources have bottomless holes instead of the geometry considered here. Nevertheless, it is believed that the results obtained here should be similar to the bottomless hole geometry, especially for high aspect ratio features.

B. Monte Carlo simulation

Ions with the appropriate energy and angular distribution^{8,12} were launched at a plane near the sheath edge. The launch plane was such that the potential distribution was essentially one-dimensional on that plane, i.e., the potential at that location was not perturbed by the presence of the trench. Ions were then accelerated by the spatially nonuniform electric field determined by the fluid simulation. The three spatial coordinates and three velocity components were tracked in time by a fourth order Runge–Kutta scheme. During their transit through the sheath, ions can interact with the background neutral gas, i.e., they can suffer elastic scattering or charge-exchange collisions. A constant total cross section was used to evaluate the distance between collision events by the null collision method.¹³ Ion-neutral collision cross sections were taken from the literature (Ref. 10, p. 78). Elastic scattering was treated as a hard sphere collision. For charge exchange collisions, the (fast) ion and (slow) neutral switched identity (i.e., became fast neutral and slow ion, respectively) without altering their precollision velocity vector (resonant process). The resulting energetic (fast) neutrals could suffer elastic scattering further on, which was also treated as a hard sphere collision. Fast neutrals, however, were primarily generated by neutralization of ions on the substrate (wall).

Energetic particle (ions or fast neutrals) scattering on a surface is quite complicated.¹⁴ Incidence angle, energy, and surface condition (roughness, contamination) all play a role. Several experimental and/or computational studies^{15–18} have been reported on the impact of energetic ($1\ \text{eV} < \varepsilon_i < 1\ \text{keV}$) ions on surfaces. The energy and angular distributions of reflected species are still the subject of investigations. The employed model for surface scattering is the simplest possible, consistent with current knowledge. Ions were assumed to neutralize upon collision with the wall (Ref. 10, p. 280) and to reflect specularly (i.e., incidence angle $\theta_i =$ reflection angle θ_r). Specular reflection was assumed in the absence of any data pertaining to the system at hand. Helmer and Graves¹⁷ conducted molecular dynamics simulations of low energy (20–100 eV) Ar^+ impact on silicon sur-

TABLE I. Base parameter values used for simulation.

| | |
|---|---------|
| Electron temperature | 3.7 eV |
| Ion temperature ^a | 0.1 eV |
| Transverse ion temperature ^a | 0.1 eV |
| Gas temperature | 0.05 eV |
| Gas pressure | 5 mTorr |
| Substrate material | Fe |

^aUsed for Monte Carlo simulation only.

faces. The details of scattering depended on ion energy and incidence angle, as well as the surface conditions (degree of surface chlorination, surface roughness). Nevertheless, specular reflection is very likely at near grazing angle collisions. To calculate the energy transfer, a binary collision model with two half-scatterings was employed.¹⁷

$$\sqrt{\frac{\varepsilon_r}{\varepsilon_i}}(\chi) = \left(\frac{\mu}{\mu+1}\right)^2 \left(\cos \chi_{1/2} + \sqrt{\frac{1}{\mu^2} - \sin^2 \chi_{1/2}}\right)^2, \quad (1)$$

where ε_r and ε_i are the kinetic energy of reflected and incident particle, respectively. The mass ratio $\mu \equiv m_{\text{Ar}}/m_{\text{Fe}} = 0.72$. This model assumes that the incident particle experiences two consecutive binary collisions with surface atoms before being released from the surface. The scattering angle was assumed to be the same for both collisions. The half-scattering angle $\chi_{1/2}$ is therefore

$$\chi_{1/2} = \frac{\chi}{2} = \frac{\pi - \theta_i - \theta_r}{2} = \frac{\pi}{2} - \theta_i. \quad (2)$$

Helmer and Graves¹⁷ observed that the average energy of reflected Ar can be reasonably estimated by the binary collision model.

III. RESULTS AND DISCUSSION

A. Electric field and ion distributions

The plasma density n_o and electric potential Φ_o at the upper boundary of Fig. 1 were the main parameters varied in this study. These parameters were used to control the self-consistent sheath thickness. The wall potential was always at $\Phi_W = 0$. Other parameters were fixed at base values shown in Table I. Unless mentioned otherwise, a 500 μm wide and 2500 μm deep (aspect ratio $H/D = 5$) trench in Fe was used as base geometry for simulations. Selected cases of simulation conditions are shown in Table II, where the sheath thickness and the ion flux on a flat wall are also shown. The range of L_{sh}/D studied was from 0.226 to 2.13.

The electric field vector profiles near the mouth of a trench (500 μm wide and 2500 μm deep) are shown in Fig. 2. Cases (a)–(c) of Fig. 2 correspond, respectively, to cases (a)–(c) of Table II. The electric field is very weak outside the sheath and picks up in strength as one enters the sheath near the wall. The electric field vectors are nearly vertical away from the trench, but diverge strongly near the trench. The highest electric field strength is at the corners of the trench mouth. The field divergence has direct implications for ion trajectories near the trench. Importantly, ions spend much of their sheath transit time in regions of strongly divergent fields. Thus such ions acquire a significant horizontal velocity component, impact the trench sidewall, and turn into energetic neutrals. When the sheath is relatively thin [case (c)], the electric field has a stronger horizontal component, resulting in stronger divergence of ions. On the other hand, when the sheath is relatively thick [as in case (a)], ions acquire significant vertical momentum before they approach the trench mouth. Therefore more ions can arrive at the trench bottom without striking the sidewall.

Figure 3 displays ion flux profiles along the centerline ($x = 0$) of the computational domain (Fig. 1) from the upper boundary ($y = 3000 \mu\text{m}$) down to the trench bottom (y

TABLE II. Selected simulation cases. The trench used for the cases shown here was 500 μm wide and 2500 μm deep. The electric potential on the upper boundary was 100 V (dc) and the wall was grounded. Other parameters were as in Table I. The resulting sheath thickness and undisturbed ion flux were calculated on a flat wall far away from the trench, where plasma molding is absent (one-dimensional sheath). The sheath edge was defined as the position where the relative net charge, $(n_i - n_e)/n_i$, was equal to 0.01, with the densities determined by the fluid simulation.

| Case | Plasma density on upper boundary n_o (m^{-3}) | Sheath thickness L_{sh} (μm) | Sheath thickness/ trench width L_{sh}/D | Undisturbed ion flux ($\text{m}^{-2} \text{s}^{-1}$) |
|------|--|--|--|--|
| (a) | 2×10^{16} | 1064 | 2.128 | 4.707×10^{19} |
| (b) | 6×10^{16} | 632 | 1.264 | 1.324×10^{20} |
| (c) | 2×10^{17} | 352 | 0.704 | 4.480×10^{20} |
| (d) | 6×10^{17} | 206 | 0.412 | 1.305×10^{21} |
| (e) | 2×10^{18} | 113 | 0.226 | 4.383×10^{21} |

Note: The ion flux at the wall (last column of the table) is not exactly proportional to the ion density at the upper boundary (second column). Only the ion density (not the flux) was specified at the upper boundary. The ion velocity at that location was found as part of the solution. Since the sheath thickness decreased with increasing ion density, while the location of the upper boundary was always the same, the entering ions were further away from the sheath edge, as ion density was increased. This resulted in lower ion velocity at the upper boundary. Thus the flux at the wall is a sublinear function of the ion density at the upper boundary.

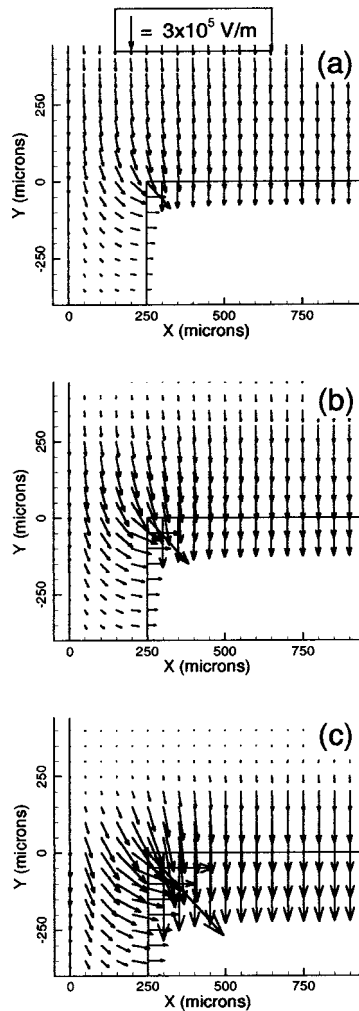


FIG. 2. Electric field vector plots near the mouth of a 500 μm wide and 2500 μm deep trench. Position $x=0$ is a plane of symmetry. (a) $L_{\text{sh}}=1064 \mu\text{m}$ ($L_{\text{sh}}/D=2.128$), (b) $L_{\text{sh}}=632 \mu\text{m}$ ($L_{\text{sh}}/D=1.264$), and (c) $L_{\text{sh}}=352 \mu\text{m}$ ($L_{\text{sh}}/D=0.704$). Cases (a)–(c) correspond to cases (a)–(c), respectively, of Table II. The potential of the upper boundary was 100 V and the wall was grounded.

$= -2500 \mu\text{m}$). For each sheath thickness shown, the ion flux was normalized by the corresponding undisturbed value (Table II). If there were no sheath disturbance, the ion flux would have been constant (at a value of 1.0). Upon entering the sheath, ions start to feel a horizontal component of the electric field, which becomes stronger as the substrate is approached. Ions are diverted by this field, strike the sidewall, and neutralize. This leads to the ion flux decreasing monotonically inside the trench. The reduction of the flux depends on the sheath thickness. As the sheath thickness increases from 113 to 1064 μm , the flux at the trench *mouth* ($y=0$) first decreases and then increases, following the trend found in a previous study.⁹ Inside the trench, the ion flux drops drastically as a function of depth. The flux reduction is stronger for thinner sheaths. When the sheath is relatively thin, ions entering the trench are more likely to diverge [Fig. 2(c)], strike the sidewall, and neutralize. As a result, a smaller ion flux is observed at the bottom. The largest normalized flux at

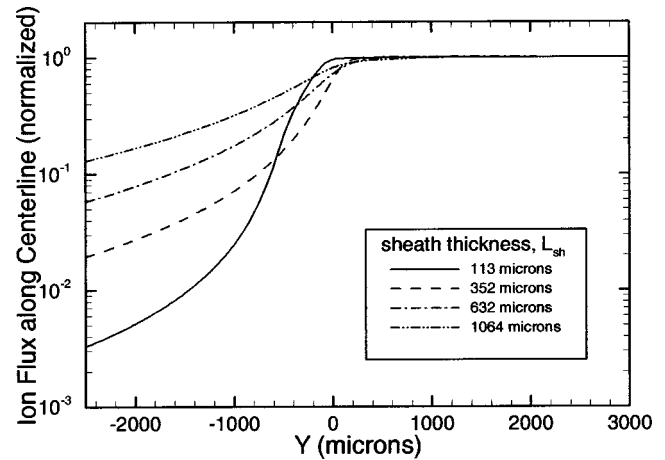


FIG. 3. Ion flux along the centerline ($x=0$) of the computational domain (Fig. 1) for different sheath thicknesses. The flux was normalized by its undisturbed value for each case, shown in Table II. The trench was 500 μm wide and 2500 μm deep. The potential of the upper boundary was 100 V and the wall was grounded.

the bottom of the deep trench is ~ 0.1 , for the thickest sheath ($L_{\text{sh}}=1064 \mu\text{m}$).

The ion flux along the contour of the trench is shown in Fig. 4. Since only the normal (to the corresponding surface) component of the flux is shown, the flux is discontinuous at the corner point Q . When the sheath is thin, a larger ion flux is found along the sidewall (PQ in inset) and, at the same time, a larger fraction of the flux is confined over a small region near the corner (point Q), where the horizontal component of the electric field (and ion divergence) is strongest. The flux becomes more uniform as plasma molding becomes

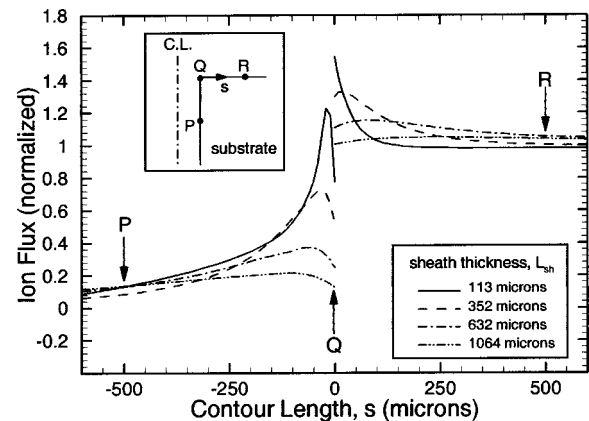


FIG. 4. Ion flux vs contour length along the surface of the trench as a function of the sheath thickness, under the conditions of Table II. The flux was normalized by the undisturbed value on a flat wall. Only the normal component of the flux is shown, i.e., $n_i v$ for horizontal surface (QR) and $n_i u$ for sidewall (PQ), where n_i is the ion density and u and v are the horizontal and vertical components of the ion fluid velocity, respectively. The contour length, s , was measured from point Q (upper corner of the trench) along the surface as displayed by the arrow of the inset. The trench was 500 μm wide and 2500 μm deep. The potential of the upper boundary was 100 V and the wall was grounded. For thicker sheaths, one has to go further out along QR to reach a normalized value of unity for the ion flux.

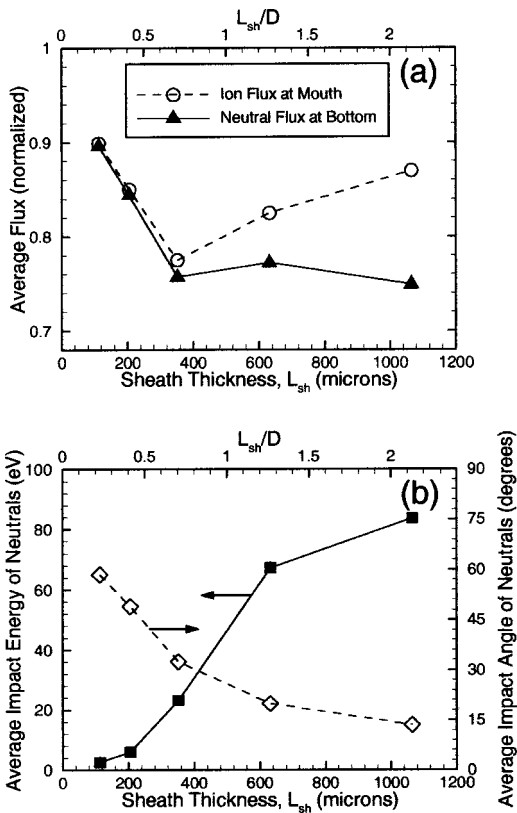


FIG. 5. (a) Average (spatially) ion flux at the trench *mouth* and average (spatially) neutral flux at the trench *bottom* as a function of sheath thickness. (b) Average (spatially) energy and impact angle of fast neutrals at the trench *bottom* as a function of sheath thickness. The fluxes were normalized by the undisturbed value of ion flux on a flat wall (see Table II). The trench was 500 μm wide and 2500 μm deep. The potential of the upper boundary was 100 V and the wall was grounded.

weaker, i.e., as the sheath thickness increases and ions become more directional along the vertical (y) axis.

B. Neutral distributions at the trench bottom

In neutral beam processing, energetic neutrals (instead of ions) promote surface reactions on target materials. In the neutral beam source described in Ref. 3, ions are thought to neutralize by grazing angle collision with the inside surface of the high aspect ratio holes of the extraction grid. Neutralized ions exiting the bottom of the holes formed an energetic neutral beam. Therefore the flux, energy, and angular distributions of energetic neutrals at the trench bottom are of great interest in the present work. The variation of (spatially) average neutral flux at the trench *bottom* as a function of the sheath thickness is shown in Fig. 5(a). For comparison, the ion flux at the trench *mouth* is also displayed. For the system pressure of 5 mTorr, the mean free path of Ar^+ ions is ~ 1 cm. Thus energetic neutrals are produced mainly by ion neutralization on the substrate surface. Therefore the ion flux at the trench mouth should be equal to the total flux of ions and energetic neutrals at the bottom, assuming no surface trapping at the Fe substrate. When the sheath is thin and most of the ions entering the trench are diverted (to strike the sidewall and neutralize), the neutral flux at the *bottom* is

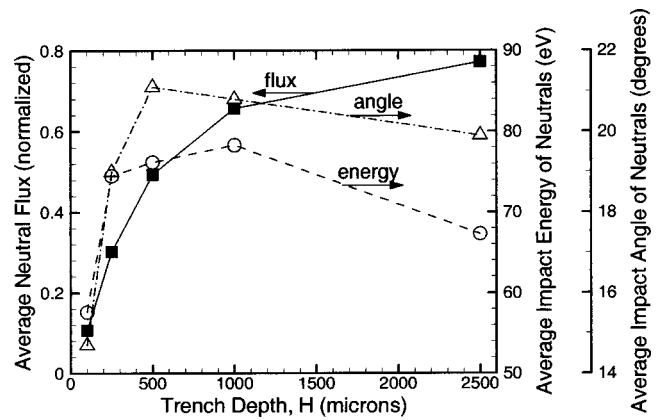


FIG. 6. Average (spatially) flux, impact energy, and impact angle (off normal) of energetic neutrals at the trench bottom vs trench depth. The flux was normalized by the undisturbed value of ion flux on a flat wall. The trench was 500 μm wide and the sheath thickness was 632 μm . The potential of the upper boundary was 100 V and the wall was grounded.

almost equal to the ion flux at the *mouth*. For thick sheaths, the ion flux at the bottom increases (~ 0.1 for $L_{sh} = 1064$ μm , see Fig. 3) and the neutral flux at the bottom tends to decrease. The (spatially) average impact energy and angle of neutrals at the trench *bottom* are shown in Fig. 5(b). When the sheath is thin, a strong horizontal component of the electric field is present, and ions are deflected to strike the sidewall at large angles (with respect to the y axis). Ions then lose a large fraction of their kinetic energy upon collision with the wall, resulting in low energy neutrals. For a thicker sheath, ions have more vertical momentum, producing fast neutrals with smaller angles and larger kinetic energies. For example, for $L_{sh} = 113$ μm , only neutrals with kinetic energy of several eV are collected at the bottom. For $L_{sh} = 1064$ μm , energetic neutrals with more than 80% of the sheath voltage (100 V in this case) impinge on the bottom surface with better directionality (impact angle is $\sim 15^\circ$ off normal). Fast neutrals with high vertical momentum are desirable for neutral beam applications. This can be achieved by increasing the sheath thickness, for a fixed trench width. However, a thicker sheath implies a smaller plasma density, and thus a smaller ion (and energetic neutral) flux (see also Table II). A way to increase sheath thickness without influencing plasma density is to apply a larger bias voltage (see Fig. 7 below). This is achievable in systems in which plasma production is decoupled from substrate bias (as in inductively coupled plasma or electron cyclotron resonance sources).

Flux, energy, and impact angle of fast neutrals at the trench *bottom* are considerably affected by the trench depth H . Figure 6 shows (spatially) average neutral distributions at the bottom of 500 μm wide trenches with different depths. The neutral flux increases with depth, in accordance with the results of Fig. 3. The average energy and angle of fast neutrals go through a shallow maximum as the depth is increased. For very thin sheaths the produced neutrals keep colliding with the sidewall during their transit toward the

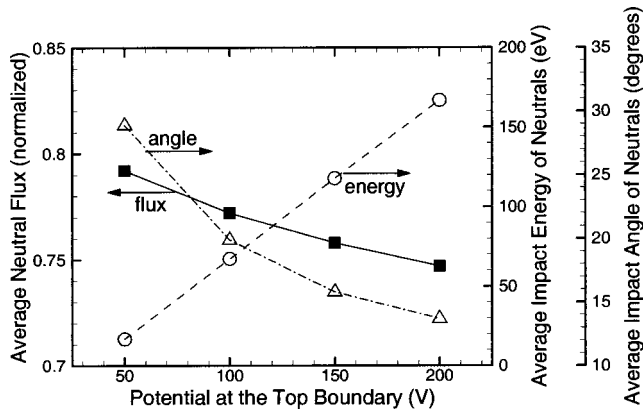


FIG. 7. Average (spatially) flux, impact energy, and impact angle (off normal) of energetic neutrals at the trench bottom vs electric potential at the upper boundary. The flux was normalized by the undisturbed value of ion flux on a flat wall. The trench was $500 \mu\text{m}$ wide and $2500 \mu\text{m}$ deep. The ion density at the upper boundary was $6 \times 10^{16} \text{m}^{-3}$.

bottom (multiple collisions), and their kinetic energy is lower.

Since the wall was always grounded (Fig. 1), the potential of the upper boundary Φ_o was essentially equal to the sheath potential (actually there is a small potential drop from the upper boundary to the sheath edge). According to Child's law, the sheath thickness scales approximately as $\Phi_o^{3/4} n_o^{-1/2}$.¹⁹ Thus plasma molding depends on the sheath potential Φ_o . Figure 7 shows (spatially) average neutral distributions at the trench *bottom* as a function of potential of the top (upper) boundary (essentially the sheath potential). The variation of neutral flux at the bottom suggests that the ion trajectory becomes more anisotropic (vertical) at higher sheath potentials. Thus fewer ions strike the sidewall, and a smaller flux of neutrals is observed when the sheath potential is increased. The enhanced ion directionality is also clearly seen in terms of the impact energy and angle of energetic neutrals. As the sheath potential is increased, higher energy neutrals impinge on the bottom at smaller angles off normal.

IV. SUMMARY AND CONCLUSIONS

A two-dimensional fluid/Monte Carlo simulation was developed to study plasma molding over deep trenches and the resulting ion and energetic (fast) neutral distributions, with emphasis on neutral beam sources. The self-consistent fluid simulation included the ion mass and momentum continuity equations, coupled to the Poisson equation for the electric potential. Using the electric field profiles from the self-consistent fluid simulation, ions and energetic neutrals (resulting mainly by ion neutralization on the sidewall) were followed by the Monte Carlo simulation. With these simulation procedures, ion flow, and ion and energetic neutral distributions in deep trenches were predicted.

The dominant energetic species at the bottom of a high aspect ratio trench ($500 \mu\text{m}$ wide and $2500 \mu\text{m}$ deep) were neutrals. When the sheath was thin compared to the trench

width, most ions entering the trench mouth struck the sidewall and reflected as fast neutrals. As the sheath thickness increased, the ion flow became more directional (along the vertical), and more ion flux was observed at the trench bottom, with a corresponding reduction in the flux of fast neutrals. However, the energy and directionality of the fast neutrals increased progressively as the sheath thickness was increased. Applying a larger bias potential was effective in making the ion flow more directional and produce a neutral beam with higher energy and directionality.

The results of this study are not applicable to very small (submicron) features often encountered in microelectronics. For such features, plasma molding is absent since the feature size is much smaller than the sheath thickness. Thus ions accelerate along the normal to the surface (one-dimensional electric field) for most of the sheath except for a few microns near the feature, where ions experience a multidimensional field. Therefore ion deflection should not be as important, assuming no surface charging. This is in contrast to the present work where a significant fraction of the oncoming ions are deflected to the sidewalls of the feature because of plasma molding over the (large) feature.

ACKNOWLEDGMENTS

Financial support by Sandia National Laboratories, the National Science Foundation (CTS-0072854), the National Institute of Standards and Technology, and the Institute of Space Systems Operations (ISSO) of the University of Houston is gratefully acknowledged.

- ¹I. W. Rangelow and H. Loschner, *J. Vac. Sci. Technol. B* **13**, 2394 (1995).
- ²*Handbook of Plasma Processing Technology*, edited by S. M. Rossnagel, J. J. Cuomo, and W. D. Westwood (Noyes, Park Ridge, NJ, 1990).
- ³S. Panda, D. J. Economou, and L. Chen, *J. Vac. Sci. Technol. A* **19**, 398 (2001).
- ⁴G. S. Hwang and K. P. Giapis, *J. Appl. Phys.* **82**, 566 (1997).
- ⁵T. Kinoshita, M. Hane, and J. P. McVittie, *J. Vac. Sci. Technol. B* **14**, 560 (1996).
- ⁶S. Samukawa, K. Sakamoto, and K. Ichiki, *Jpn. J. Appl. Phys., Part 2* **40**, L997 (2001); *J. Vac. Sci. Technol. A* **20**, 1566 (2002).
- ⁷J. R. Woodworth, P. A. Miller, R. J. Shul, I. C. Abraham, B. P. Aragon, T. W. Hamilton, C. G. Willison, D. Kim, and D. J. Economou, *J. Vac. Sci. Technol. A* **21**, 147 (2003).
- ⁸D. Kim and D. J. Economou, *IEEE Trans. Plasma Sci.* **30**, 2048 (2002).
- ⁹D. Kim, D. J. Economou, J. R. Woodworth, P. A. Miller, R. J. Shul, B. P. Aragon, T. W. Hamilton, and C. G. Willison, *IEEE Trans Plasma Sci.* (to be published).
- ¹⁰M. A. Lieberman and A. J. Lichtenberg, *Principles of Plasma Discharges and Materials Processing* (Wiley, New York, 1994).
- ¹¹J. P. Boris and D. L. Book, *J. Comput. Phys.* **11**, 38 (1973).
- ¹²K.-U. Riemann, *Phys. Fluids* **24**, 2163 (1982); J. R. Woodworth, M. E. Riley, P. A. Miller, G. A. Hebner, and T. W. Hamilton, *J. Appl. Phys.* **81**, 5950 (1997).
- ¹³C. K. Birdsall, *IEEE Trans. Plasma Sci.* **19**, 65 (1991).
- ¹⁴H. Niehus, W. Heiland, and E. Taglauer, *Surf. Sci. Rep.* **17**, 213 (1993).
- ¹⁵S. R. Kasi, M. A. Kilburn, H. Kang, J. W. Rabalais, L. Tavernini, and P. Hochmann, *J. Chem. Phys.* **88**, 5902 (1988).
- ¹⁶G. S. Hwang, C. M. Anderson, M. J. Gordon, T. A. Moore, T. K. Minton, and K. P. Giapis, *Phys. Rev. Lett.* **77**, 3049 (1996).
- ¹⁷B. A. Helmer and D. B. Graves, *J. Vac. Sci. Technol. A* **16**, 3502 (1998).
- ¹⁸W. Choi, C. Kim, and H. Kang, *Surf. Sci.* **281**, 323 (1993).
- ¹⁹C. D. Child, *Phys. Rev.* **32**, 492 (1911).